

Near-field Hybrid Beamforming for Terahertz-band Integrated Sensing and Communications

Ahmet M. Elbir^{†,†}, Abdulkadir Celik[†] and Ahmed M. Eltawil[†]

[†]University of Luxembourg, Luxembourg

⁺King Abdullah University of Science and Technology, Saudi Arabia

E-mail: ahmetmelbir@ieee.org, abdulcadir.celik@kaust.edu.sa, ahmed.eltawil@kaust.edu.sa

Abstract—Terahertz (THz) band communications and integrated sensing and communications (ISAC) are two main facets of the sixth generation wireless networks. In order to compensate the severe attenuation, the THz wireless systems employ large arrays, wherein the near-field beam-squint severely degrades the beamforming accuracy. Contrary to prior works that examine only either narrowband ISAC beamforming or far-field models, we introduce an alternating optimization technique for hybrid beamforming design in near-field THz-ISAC scenario. We also propose an efficient approach to compensate near-field beam-squint via baseband beamformers. Via numerical simulations, we show that the proposed approach achieves satisfactory spectral efficiency performance while accurately estimating the near-field beamformers and mitigating the beam-squint without additional hardware components.

Index Terms—Integrated sensing and communications, massive MIMO, terahertz, near-field, beamforming

I. INTRODUCTION

Integrated sensing and communications (ISAC) has emerged as one of the pivotal technologies of future sixth generation (6G) wireless networks, enabling synergistic access to the scarce radio spectrum on an integrated hardware platform [1, 2]. In particular, as the allocation of the spectrum beyond 100 GHz is underway, specifically in the terahertz (THz) band, ISAC is currently witnessing frantic research endeavors to simultaneously achieve high-resolution sensing and ultrahigh-speed communications system architecture at the THz frequencies [2, 3].

Signal processing at THz-band confronts multiple impediments, such as severe path loss, limited transmission distance, and *beam-squint*. To surmount these challenges at reduced hardware costs, hybrid analog and digital beamforming architectures are employed in a massive multiple-input multiple-output (MIMO) array configuration [4, 5]. For higher spectral efficiency (SE) and lower complexity, massive MIMO systems employ wideband signal processing, wherein subcarrier-dependent (SD) baseband and subcarrier-independent (SI) analog beamformers are adopted. In particular, the weights of the analog beamformers are subject to a single (sub-)carrier frequency [6]. Therefore, the beam generated across the subcarriers points towards disparate directions, engendering beam-squint phenomenon [7, 8]. Compared to millimeter-wave (mm-Wave) frequencies, beam-

squint’s ramifications are more acute in THz massive MIMO because of wider system bandwidths in the latter [8, 9]. As such, addressing beam-squint is imperative for ensuring reliable system performance. Existing techniques to compensate for the impact of beam-squint mostly employ additional hardware components, e.g., time-delayer (TD) networks [8, 10] and SD phase shifter networks [11] to virtually realize SD analog beamformers. However, these approaches are inefficient in terms of cost and power [2]. It merits noting that beam-squint compensation does not necessitate additional hardware components for estimation of the communications channel and radar target direction-of-arrival, which can be handled in the digital domain, wherein the generation of SD analog beamformers is possible. Nevertheless, supplementary (analog) hardware is required for hybrid (analog/digital) beamformer design [5, 12].

Beside beam-squint, another formidable challenge in THz-band signal processing is short-transmission distance, which may cause the signal wavefront at the receive to become spherical in near-field (see, e.g., Fig. 1). In particular, the plane wavefront is spherical in the near-field when the transmission range is shorter than the Fraunhofer distance [13]. As a result, the beamforming algorithms must accommodate the near-field model, which depends on both direction and range information for accurate signal processing [2]. Among the works investigating the near-field signal model, [14–16] consider the near-field scenario, while neglecting the effect of beam-squint and focusing solely on mm-Wave scenarios. On the other hand, several methods have been proposed to compensate the far-field beam-squint for both THz channel estimation [17, 18] and beamforming [3, 19] applications. Furthermore, near-field THz channel estimation is explored in [20, 21], wherein an orthogonal matching pursuit (OMP)-based approach is proposed. The near-field ISAC scenario is investigated in [22], albeit exclusively for narrowband systems that do not account for the impact of beam-squint. Specifically, [22] considers a near-field multiple signal classification (MUSIC) algorithm to estimate the direction and ranges of radar targets and communication users. Nevertheless, near-field ISAC hybrid beamforming in the presence of beam-squint remains relatively unexamined.

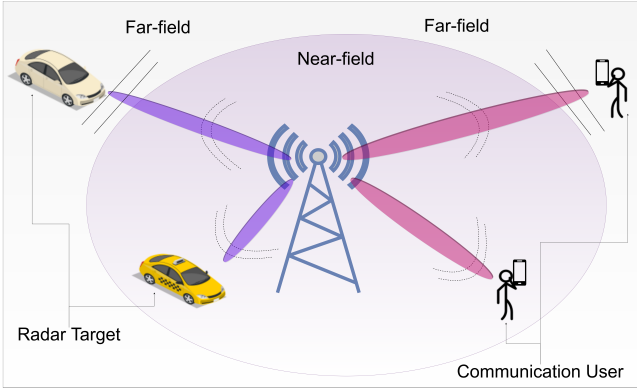


Fig. 1. Near-field ISAC scenario, wherein received signal wavefront for the communication user/targets in far-field (near-field) is plane-wave (spherical-wave).

In this paper, near-field hybrid beamforming approach is proposed for the THz-ISAC scenario. We first introduce the system model for both communications and sensing signal acquisition. Subsequently, the near-field array model and near-field beam-squint are introduced. In order to design the hybrid beamformers, an alternating algorithm is devised. Initially, a dictionary of near-field steering vectors is employed to estimate the analog beamformer. Then, the baseband beamformer and the joint radar-communications (JRC) beamformers are estimated. Finally, we introduce an efficient approach to compensate beam-squint in the baseband rather than designing SD analog beamformers [11] or TD networks [8, 10], which are hardware-inefficient. Specifically, we design a beam-squint-aware (BSA) baseband beamformer by matching the SI hybrid beamformer to the SD one. Therefore, the effect of beam-squint is conveyed from analog domain to the baseband.

Notation: Throughout the paper, $(\cdot)^T$ and $(\cdot)^H$ denote the transpose and conjugate transpose operations, respectively. For a matrix \mathbf{A} and vector \mathbf{a} ; $[\mathbf{A}]_{i,j}$, $[\mathbf{A}]_k$ and $[\mathbf{a}]_l$ correspond to the (i, j) -th entry, k -th column and l -th entry, respectively. An $N \times N$ identity matrix is represented by \mathbf{I}_N . The pulse-shaping function is represented by $\text{sinc}(t) = \frac{\pi t}{t}$. We denote $\|\cdot\|_2$ and $\|\cdot\|_{\mathcal{F}}$ as the l_2 -norm and Frobenius norm, respectively.

II. SYSTEM MODEL & PROBLEM FORMULATION

Consider a wideband transmitter design problem in an ISAC scenario with a communication user and K radar targets located in the near-field of the base station (BS) as illustrated in Fig. 1. The dual-function BS jointly communicate with the communication user and sense the radar targets via probing signals with N_T antennas over M subcarriers. The user has N_R antennas, for which N_S data symbols $\mathbf{s}[m] = [s_1[m], \dots, s_{N_S}[m]]^T \in \mathbb{C}^{N_S}$ are transmitted, where $\mathbb{E}\{\mathbf{s}[m]\mathbf{s}^H[m]\} = 1/N_S \mathbf{I}_{N_S}$.

A. Communications Model

The BS aims to transmit the data symbol vector $\mathbf{s}[m] \in \mathbb{C}^{N_S}$ toward the communications user. Thus, the BS first applies the SD baseband beamformer $\mathbf{F}_{\text{BB}}[m] \in \mathbb{C}^{N_{\text{RF}} \times N_S}$. Then, M -point inverse fast Fourier transform (IFFT) is applied to convert the signal to time-domain, and the cyclic prefix (CP) is added. Finally, the SI analog beamformer $\mathbf{F}_{\text{RF}} \in \mathbb{C}^{N_T \times N_{\text{RF}}}$ is applied, and the $N_T \times 1$ transmit signal becomes

$$\mathbf{x}[m] = \mathbf{F}_{\text{RF}} \mathbf{F}_{\text{BB}}[m] \mathbf{s}[m], \quad (1)$$

where the analog beamformer \mathbf{F}_{RF} has constant-modulus constraint, i.e., $|\mathbf{F}_{\text{RF}}[i,j]| = 1/\sqrt{N_T}$ for $i = 1, \dots, N_T$, $j = 1, \dots, N_{\text{RF}}$. Furthermore, we have $\sum_{m=1}^M \|\mathbf{F}_{\text{RF}} \mathbf{F}_{\text{BB}}[m]\|_{\mathcal{F}}^2 = MN_S$ to account for the total power constraint.

1) *THz Channel Model:* In this study, we employ Saleh-Valenzuela (S-V) multipath channel model, which is the superposition of received non-LoS (NLoS) paths to model the THz channel [23, 24]. Compared to the mmWave channel, the THz channel involves limited reflected paths and negligible scattering [23, 25]. For massive MIMO systems, approximately 5 paths survive at 0.3 THz compared to approximately 8 paths at 60 GHz [25]. Especially for outdoor applications, multipath channel models are widely used to represent the THz channel for a more general scenario [23, 25]. Hence, in this work, we consider a general scenario, wherein the delay- \bar{d} $N_R \times N_T$ MIMO communications channel involving L NLoS paths is given in discrete-time domain as

$$\tilde{\mathbf{H}}(\bar{d}) = \sum_{l=1}^L \gamma_l \text{sinc}(\bar{d} - B\tau_l) \mathbf{a}_{\text{R}}(\theta_l, \rho_l) \mathbf{a}_{\text{T}}^H(\phi_l, r_l), \quad (2)$$

where $\gamma_l \in \mathbb{C}$ denotes the channel path gain, B represents the system bandwidth and τ_l is the time delay of the l -th path. θ_l (ρ_l) and ϕ_l (r_l) denote the physical DoA and direction-of-departure (DoD) angles (ranges) of the scattering paths between the user and the BS, respectively, where $\theta_l = \sin \tilde{\theta}_l$, $\phi_l = \sin \tilde{\phi}_l$ and $\tilde{\theta}_l, \tilde{\phi}_l \in [-\frac{\pi}{2}, \frac{\pi}{2}]$. Then, the corresponding receive and transmit steering vectors are defined as $\mathbf{a}_{\text{R}}(\theta_l, \rho_l) \in \mathbb{C}^{N_R}$ and $\mathbf{a}_{\text{T}}(\phi_l, r_l) \in \mathbb{C}^{N_T}$, respectively. Performing M -point FFT of the delay- \bar{d} channel given in (2) yields

$$\mathbf{H}[m] = \sum_{\bar{d}=1}^{\bar{D}-1} \tilde{\mathbf{H}}(\bar{d}) e^{-j \frac{2\pi m}{M} \bar{d}}, \quad (3)$$

where $\bar{D} \leq M$ is the CP length. Then, the $N_R \times N_T$ channel matrix in frequency domain is represented by

$$\mathbf{H}[m] = \sum_{l=1}^L \gamma_l \mathbf{a}_{\text{R}}(\bar{\theta}_{l,m}, \bar{\rho}_{l,m}) \mathbf{a}_{\text{T}}^H(\bar{\phi}_{l,m}, \bar{r}_{l,m}) e^{-j 2\pi \tau_l f_m}, \quad (4)$$

where $\bar{\theta}_{l,m}$ ($\bar{\rho}_{l,m}$) and $\bar{\phi}_{l,m}$ ($\bar{r}_{l,m}$) denote the spatial directions (ranges), which are SD and they are deviated from the

physical directions θ_l , ϕ_l (ρ_l, r_l) in the beamspace due to beam-squint [2, 8]. On the other hand, the beam-squint-free channel matrix is

$$\bar{\mathbf{H}}[m] = \sum_{l=1}^L \gamma_l \mathbf{a}_R(\phi_l, \rho_l) \mathbf{a}_T^H(\theta_l, r_l) e^{-j2\pi r_l f_m}. \quad (5)$$

Then, the $N_R \times 1$ received signal at the communications user is

$$\mathbf{y}[m] = \mathbf{H}[m] \mathbf{F}_{RF} \mathbf{F}_{BB}[m] \mathbf{s}[m] + \mathbf{n}[m], \quad (6)$$

where $\mathbf{n}[m] \sim \mathcal{CN}(\mathbf{0}, \sigma_n^2 \mathbf{I}_{N_R}) \in \mathbb{C}^{N_R}$ represents the temporarily and spatially additive white Gaussian noise vector.

2) *Beam-Squint Effect*: In wideband transmission, the prevalent assumption is the employment of a monochromatic wavelength across all subcarriers, delineated as $\lambda_1 = \dots \lambda_M = \frac{c_0}{f_c}$, wherein c_0 signifies the speed of light and f_c represents the carrier frequency. However, the utilization of a singular analog beamformer renders this monochromatic wavelength assumption inapplicable, culminating in the formation of squinted beams that orient toward disparate spatial directions and ranges [2, 8]. Presuming an analogous beamforming architecture is employed at the user end (i.e., SI analog beamformer with SD digital beamformers), the high-frequency operation at THz implies the presence of close-proximity users in the near-field region, where planar wave propagation is not valid. At ranges shorter than the Fraunhofer distance $d_F = \frac{2D^2}{\lambda}$, where D is the array aperture and $\lambda = \frac{c_0}{f_c}$ is the wavelength, the near-field wavefront exhibits spherical nature [7, 13]. For a uniform linear array (ULA), the array aperture is $D = (N-1)d$, where $d = \frac{\lambda}{2}$ is the element spacing. In the THz spectrum, it is imperative to employ a near-field signal model because $r_l < d_F$. For instance, when $f_c = 300$ GHz and $N = 256$, the Fraunhofer distance is $d_F = 32.76$ m.

Taking into account the spherical-wave model [13, 20, 26], we define the near-field steering vector $\mathbf{a}_T(\phi_l, r_l) \in \mathbb{C}^{N_T}$ corresponding to the physical DoA ϕ_l and range r_l as

$$\mathbf{a}_T(\phi_l, r_l) = \frac{1}{\sqrt{N_T}} [e^{-j2\pi \frac{d}{\lambda} r_l^{(1)}}, \dots, e^{-j2\pi \frac{d}{\lambda} r_l^{(N_T)}}]^T, \quad (7)$$

where $r_l^{(n)}$ is the distance between the l -th path scatterer and the n -th antenna as

$$r_l^{(n)} = (r_l^2 + 2(n-1)^2 d^2 - 2r_l(n-1)d\phi_l)^{\frac{1}{2}}. \quad (8)$$

Following the Fresnel approximation [20, 26], (8) becomes

$$r_l^{(n)} \approx r_l - (n-1)d\phi_l + (n-1)^2 d^2 \zeta_l, \quad (9)$$

where $\zeta_l = \frac{1-\phi_l^2}{2r_l}$. Rewrite (7) as

$$\mathbf{a}_T(\phi_l, r_l) \approx e^{-j2\pi \frac{f_c}{c_0} r_l} \tilde{\mathbf{a}}_T(\phi_l, r_l), \quad (10)$$

where the n -th element of $\tilde{\mathbf{a}}_T(\phi_l, r_l) \in \mathbb{C}^{N_T}$ is

$$[\tilde{\mathbf{a}}_T(\phi_l, r_l)]_n = e^{j2\pi \frac{f_c}{c_0} ((n-1)d\phi_l - (n-1)^2 d^2 \zeta_l)}. \quad (11)$$

The steering vector in (10) corresponds to the physical location (ϕ_l, r_l) . This deviates to the spatial location $(\bar{\phi}_{m,l}, \bar{r}_{m,l})$ in the beamspace because of the absence of SD analog beamformers. Then, the n -th entry of the deviated steering vector in (11) for the spatial location is

$$[\tilde{\mathbf{a}}_T(\bar{\phi}_{m,l}, \bar{r}_{m,l})]_n = e^{j2\pi \frac{f_m}{c_0} ((n-1)d\bar{\phi}_{m,l} - (n-1)^2 d^2 \bar{\zeta}_{m,l})}. \quad (12)$$

Theorem 1. Denote $\mathbf{u} \in \mathbb{C}^{N_T}$ and $\mathbf{v}_m \in \mathbb{C}^{N_T}$ as the arbitrary near-field steering vectors corresponding to the physical (i.e., $\{\phi_l, r_l\}$) and spatial (i.e., $\{\bar{\phi}_{m,l}, \bar{r}_{m,l}\}$) locations given in (11) and (12), respectively. Then, in spatial domain at subcarrier frequency f_m , the array gain achieved by $\mathbf{u}^H \mathbf{v}_m$ is maximized and the generated beam is focused at the location $\{\bar{\phi}_{m,l}, \bar{r}_{m,l}\}$ such that

$$\bar{\phi}_{m,l} = \eta_m \phi_l, \quad \bar{r}_{m,l} = \frac{1 - \eta_m^2 \phi_l^2}{\eta_m (1 - \phi_l^2)} r_l, \quad (13)$$

where $\eta_m = \frac{f_c}{f_m}$ represents the proportional deviation of DoA/ranges.

Proof. Please see [20]. ■

Following (9) and (13), we define near-field beam-squint in terms of DoAs and ranges as, respectively,

$$\Delta(\phi_l, m) = \bar{\phi}_{m,l} - \phi_l = (\eta_m - 1)\phi_l, \quad (14)$$

and $\Delta(r_l, m) = \bar{r}_{m,l} - r_l = (\eta_m - 1)r_l$, i.e.,

$$\Delta(r_l, m) = (\eta_m - 1) \frac{1 - \eta_m^2 \phi_l^2}{\eta_m (1 - \phi_l^2)} r_l. \quad (15)$$

B. Radar Model

The aim of the radar sensing task is to achieve the highest SNR toward targets. Denote the estimate of the k -th target direction and range by Φ_k and r_k , which can be estimated during the search phase of the radar, e.g., MUSIC algorithm [12]. Then, we select the radar-only beamformer as

$$\mathbf{F}_R = [\mathbf{a}_T(\Phi_1, r_1), \dots, \mathbf{a}_T(\Phi_K, r_K)] \in \mathbb{C}^{N_T \times K}. \quad (16)$$

The proposed ISAC beamformer aims to generate multiple beams toward both radar targets and the communication user. This allows us to maintain the communication between the user and the BS while tracking the radar targets, of which the initial directions/ranges are estimated. Using the hybrid beamforming structure, the beam pattern of the radar for $\Phi \in [-\frac{\pi}{2}, \frac{\pi}{2}]$ and $r \in [0, d_F]$ is

$$B_m(\Phi, r) = \text{Trace}\{\mathbf{a}_T^H(\Phi, r) \mathbf{R}_x[m] \mathbf{a}_T(\Phi, r)\}, \quad (17)$$

where $\mathbf{a}_T(\Phi, r) \in \mathbb{C}^{N_T}$ denotes the steering vector corresponding to arbitrary direction Φ and range r , and $\mathbf{R}_x[m] \in \mathbb{C}^{N_T \times N_T}$ is the covariance of the transmit signal as

$$\begin{aligned} \mathbf{R}_x[m] &= \mathbb{E}\{\mathbf{x}[m] \mathbf{x}^H[m]\} \\ &= \mathbf{F}_{RF} \mathbf{F}_{BB}[m] \mathbb{E}\{\mathbf{s}[m] \mathbf{s}^H[m]\} \mathbf{F}_{BB}^H[m] \mathbf{F}_{RF}^H \\ &= \frac{1}{N_S} \mathbf{F}_{RF} \mathbf{F}_{BB}[m] \mathbf{F}_{BB}^H[m] \mathbf{F}_{RF}^H. \end{aligned} \quad (18)$$

To simultaneously obtain the desired beam pattern for the radar target and provide satisfactory communications performance, the hybrid beamformer $\mathbf{F}_{\text{RF}}\mathbf{F}_{\text{BB}}[m]$ should be designed accordingly.

C. Problem Formulation

Our aim in this work is to design the ISAC hybrid beamformer $\mathbf{F}_{\text{RF}}\mathbf{F}_{\text{BB}}[m]$ while mitigating the impact of near-field beam-squint. The design problem maximizes the SE of the overall system, which can be recast via minimizing the Euclidean distance between the hybrid beamformer $\mathbf{F}_{\text{RF}}\mathbf{F}_{\text{BB}}[m]$ and the unconstrained JRC beamformer $\mathbf{F}_{\text{CR}}[m]$ [3, 4]. The JRC beamformer is defined as

$$\mathbf{F}_{\text{CR}}[m] = \varepsilon \mathbf{F}_{\text{opt}}[m] + (1 - \varepsilon) \mathbf{F}_{\text{R}} \mathbf{\Pi}[m], \quad (19)$$

where $\mathbf{F}_{\text{opt}}[m] \in \mathbb{C}^{N_{\text{T}} \times N_{\text{S}}}$ is the unconstrained communications-only beamformer, which can be obtained through the singular value decomposition (SVD) of $\mathbf{H}[m]$ [4]. $\mathbf{\Pi}[m] \in \mathbb{C}^{K \times N_{\text{S}}}$ is a unitary matrix providing the change of dimensions between \mathbf{F}_{R} and $\mathbf{F}_{\text{opt}}[m]$. In (19), $0 \leq \varepsilon \leq 1$ represents the trade-off parameter between the radar and communications tasks. In particular, $\varepsilon = 1$ ($\varepsilon = 0$) corresponds to the communications-only (radar-only) design. In ISAC, ε controls the trade-off between the accuracy/prominence of sensing and communications tasks [2]. Now, the optimization problem becomes

$$\begin{aligned} & \underset{\mathbf{F}_{\text{RF}}, \mathbf{F}_{\text{BB}}[m], \mathbf{\Pi}[m]}{\text{minimize}} \sum_{m=1}^M \|\mathbf{F}_{\text{RF}}\mathbf{F}_{\text{BB}}[m] - \mathbf{F}_{\text{CR}}[m]\|_{\mathcal{F}} \\ & \text{subject to: } |[\mathbf{F}_{\text{RF}}]_{i,j}| = 1/\sqrt{N_{\text{T}}} \\ & \sum_{m=1}^M \|\mathbf{F}_{\text{RF}}\mathbf{F}_{\text{BB}}[m]\|_{\mathcal{F}} = MN_{\text{S}} \\ & \mathbf{\Pi}[m]\mathbf{\Pi}^{\text{H}}[m] = \mathbf{I}_K. \end{aligned} \quad (20)$$

The above optimization problem is difficult to solve due to non-convex constraints, e.g., unit-modulus constraint and it involves multiple unknowns \mathbf{F}_{RF} , $\mathbf{F}_{\text{BB}}[m]$ and $\mathbf{\Pi}[m]$. In order to provide an effective solution, we follow an alternating optimization approach, wherein the beamformers are optimized one-by-one while the other term is fixed. Specifically, \mathbf{F}_{RF} is first estimated via an OMP-based approach, wherein the columns of \mathbf{F}_{RF} are selected from a dictionary of near-field steering vectors. Next, the baseband beamformer $\mathbf{F}_{\text{BB}}[m]$ and $\mathbf{\Pi}[m]$ are estimated. Finally, a BSA baseband beamformer is designed for beam-squint compensation.

III. HYBRID BEAMFORMER DESIGN

In order to solve (20) effectively, we propose an alternating algorithm to efficiently find the unknowns \mathbf{F}_{RF} , $\mathbf{F}_{\text{BB}}[m]$, $\mathbf{\Pi}[m]$. Thus, we first introduce an OMP based approach, wherein the analog beamformer \mathbf{F}_{RF} is

designed, respectively, from the columns of the dictionary matrix

$$\mathbf{D} = [\mathbf{a}_{\text{T}}(\phi_1, r_1), \dots, \mathbf{a}_{\text{T}}(\phi_N, r_N)] \in \mathbb{C}^{N_{\text{T}} \times N}, \quad (21)$$

where N is the grid size of the dictionary with $\phi_n \in [-1, 1]$, $r_n \in (0, d_{\text{F}}]$. Then, the columns of the analog beamformer \mathbf{F}_{RF} are selected from the columns of $\mathbf{D}[m]$ as $\mathbf{a}_{\text{T}}(\phi_{p^*}, r_{p^*})$, for $\ell = 1, \dots, N_{\text{RF}}$ where

$$p^* = \underset{p \in \{1, \dots, N\}}{\text{argmax}} \sum_{m=1}^M \left| \left[\mathbf{\Psi}[m] \mathbf{\Psi}^{\text{H}}[m] \right]_{p,p} \right|, \quad (22)$$

where $\mathbf{\Psi}[m] = \mathbf{a}_{\text{T}}^{\text{H}}(\phi_p, r_p) \mathbf{F}_{\text{CR}}[m]$. Once the analog beamformer \mathbf{F}_{RF} is obtained and by using $\mathbf{F}_{\text{CR}}[m]$, the baseband beamformer is given by

$$\mathbf{F}_{\text{BB}}[m] = \mathbf{F}_{\text{RF}}^{\dagger} \mathbf{F}_{\text{CR}}[m], \quad (23)$$

which is then normalized as $\mathbf{F}_{\text{BB}}[m] = \frac{\sqrt{N_{\text{S}}} \mathbf{F}_{\text{RF}}^{\dagger} \mathbf{F}_{\text{CR}}[m]}{\|\mathbf{F}_{\text{RF}} \mathbf{F}_{\text{BB}}[m]\|_{\mathcal{F}}}$. The JRC beamformer is composed of the auxiliary matrix $\mathbf{\Pi}[m]$, which can be optimized as

$$\begin{aligned} & \underset{\mathbf{\Pi}}{\text{minimize}} \|\mathbf{F}_{\text{RF}} \bar{\mathbf{F}}_{\text{BB}} - \mathbf{F}_{\text{CR}}\|_{\mathcal{F}}^2 \\ & \text{subject to: } \bar{\mathbf{\Pi}} \bar{\mathbf{\Pi}}^{\text{H}} = \mathbf{I}_K, \end{aligned} \quad (24)$$

where $\bar{\mathbf{F}}_{\text{BB}} = [\mathbf{F}_{\text{BB}}[1], \dots, \mathbf{F}_{\text{BB}}[M]]$, $\bar{\mathbf{F}}_{\text{CR}} = [\mathbf{F}_{\text{CR}}[1], \dots, \mathbf{F}_{\text{CR}}[M]]$ and $\bar{\mathbf{\Pi}} = [\mathbf{\Pi}[1], \dots, \mathbf{\Pi}[M]]$ are $N_{\text{RF}} \times MN_{\text{S}}$, $N_{\text{T}} \times MN_{\text{S}}$ and $K \times MN_{\text{S}}$ matrices composed of information corresponding to all subcarriers, respectively. The solution to the problem in (24) can be found via SVD of the $K \times MN_{\text{S}}$ matrix $\mathbf{F}_{\text{R}}^{\text{H}} \mathbf{F}_{\text{RF}} \bar{\mathbf{F}}_{\text{BB}}$ and it is given by

$$\bar{\mathbf{\Pi}} = \tilde{\mathbf{\Pi}} \tilde{\mathbf{\Sigma}} \tilde{\mathbf{V}}, \quad (25)$$

where $\tilde{\mathbf{\Pi}} \tilde{\mathbf{\Sigma}} \tilde{\mathbf{V}} = \mathbf{F}_{\text{R}}^{\text{H}} \mathbf{F}_{\text{RF}} \bar{\mathbf{F}}_{\text{BB}}$ is the SVD of the $N_{\text{RF}} \times N_{\text{S}}$ matrix $\frac{1}{1-\varepsilon} \mathbf{F}_{\text{R}}^{\text{H}} (\mathbf{F}_{\text{RF}} \bar{\mathbf{F}}_{\text{BB}} - \varepsilon \bar{\mathbf{F}}_{\text{CR}})$, and $\mathbf{I}_{K \times MN_{\text{S}}} = [\mathbf{I}_K | \mathbf{0}_{MN_{\text{S}}-K \times K}^{\text{T}}]$. Then, by estimating $\mathbf{F}_{\text{BB}}[m]$ and $\mathbf{\Pi}[m]$ iteratively, the hybrid beamformer weights are computed.

The next task is to mitigate near-field beam-squint, which can be compensated if SD analog beamformers are used. However, this approach is costly since it requires employing $MN_{\text{T}}N_{\text{RF}}$ (instead of $N_{\text{T}}N_{\text{RF}}$) phase-shifters. Instead, we propose an efficient approach, wherein the effect of beam-squint is handled in the baseband beamformer, which is SD. Therefore, the effect of beam-squint is conveyed from analog domain to baseband.

Denoted by $\check{\mathbf{F}}_{\text{RF}}[m] \in \mathbb{C}^{N_{\text{T}} \times N_{\text{RF}}}$, the SD analog beamformer that can be computed from the SI analog beamformer \mathbf{F}_{RF} as

$$\check{\mathbf{F}}_{\text{RF}}[m] = \frac{1}{\sqrt{N_{\text{T}}}} \mathbf{\Omega}[m], \quad (26)$$

where $\mathbf{\Omega}[m] \in \mathbb{C}^{N_{\text{T}} \times N_{\text{RF}}}$ includes the angle information of \mathbf{F}_{RF} as $[\mathbf{\Omega}[m]]_{i,j} = \exp\{j\eta_m \angle\{[\mathbf{F}_{\text{RF}}]_{i,j}\}\}$ for $i =$

Algorithm 1 ISAC hybrid beamforming

Input: \mathbf{D} , \mathbf{F}_R , $\mathbf{F}_{\text{opt}}[m]$, ε , η_m .

- 1: $\mathbf{F}_{\text{RF}} = \text{Empty}$, $\mathbf{F}_{\text{res}}[m] = \mathbf{F}_{\text{CR}}[m]$.
- 2: **for** $\ell = 1, \dots, N_{\text{RF}}$ **do**
- 3: $p^* = \text{argmax}_p \sum_{m=1}^M |\mathbf{a}_T^H(\phi_p, r_p) \mathbf{F}_{\text{res}}[m]|$.
- 4: $\mathbf{F}_{\text{RF}} = [\mathbf{F}_{\text{RF}} | \mathbf{a}_T(\phi_{p^*}, r_{p^*})]$.
- 5: $\mathbf{F}_{\text{BB}}[m] = (\mathbf{F}_{\text{RF}}^H \mathbf{F}_{\text{RF}})^{-1} \mathbf{F}_{\text{RF}}^H \mathbf{F}_{\text{CR}}[m]$.
- 6: Update $\mathbf{\Pi}[m]$ from (25).
- 7: Update $\mathbf{F}_{\text{CR}}[m]$ from (19).
- 8: $\mathbf{F}_{\text{res}}[m] = \frac{\mathbf{F}_{\text{CR}}[m] - \mathbf{F}_{\text{RF}} \mathbf{F}_{\text{BB}}[m]}{\|\mathbf{F}_{\text{CR}}[m] - \mathbf{F}_{\text{RF}} \mathbf{F}_{\text{BB}}[m]\|_{\mathcal{F}}}$.
- 9: **end for**
- 10: $\tilde{\mathbf{F}}_{\text{BB}}[m] = \sqrt{N_S} \frac{\mathbf{F}_{\text{BB}}[m]}{\|\mathbf{F}_{\text{RF}} \mathbf{F}_{\text{BB}}[m]\|_{\mathcal{F}}}$.
- 11: $\tilde{\mathbf{F}}_{\text{RF}}[m] = \frac{1}{\sqrt{N_T}} \mathbf{\Omega}[m]$ where $[\mathbf{\Omega}[m]]_{i,j} = \exp\{j\eta_m \angle\{\mathbf{F}_{\text{RF}}\}_{i,j}\}$.
- 12: $\tilde{\mathbf{F}}_{\text{BB}}[m] = \tilde{\mathbf{F}}_{\text{RF}}^\dagger \tilde{\mathbf{F}}_{\text{RF}}[m] \mathbf{F}_{\text{BB}}[m]$.

Return: \mathbf{F}_{RF} , $\tilde{\mathbf{F}}_{\text{BB}}[m]$.

$1, \dots, N_T$ and $j = 1, \dots, N_{\text{RF}}$. As a result, the angular deviation in \mathbf{F}_{RF} due to beam-squint is compensated with η_m .

Now, we define $\tilde{\mathbf{F}}_{\text{BB}}[m] \in \mathbb{C}^{N_{\text{RF}} \times N_S}$ as the *BSA digital beamformer* in order to achieve SD beamforming performance that can be obtained by the usage of SD analog beamformer $\tilde{\mathbf{F}}_{\text{RF}}[m]$. Hence, we aim to match the proposed *BSA hybrid beamformer* $\mathbf{F}_{\text{RF}} \tilde{\mathbf{F}}_{\text{BB}}[m]$ with the SD hybrid beamformer $\tilde{\mathbf{F}}_{\text{RF}}[m] \mathbf{F}_{\text{BB}}[m]$ as

$$\underset{\tilde{\mathbf{F}}_{\text{BB}}[m]}{\text{minimize}} \|\mathbf{F}_{\text{RF}} \tilde{\mathbf{F}}_{\text{BB}}[m] - \tilde{\mathbf{F}}_{\text{RF}}[m] \mathbf{F}_{\text{BB}}[m]\|_{\mathcal{F}}, \quad (27)$$

for which $\tilde{\mathbf{F}}_{\text{BB}}[m]$ can be obtained as

$$\tilde{\mathbf{F}}_{\text{BB}}[m] = \mathbf{F}_{\text{RF}}^\dagger \tilde{\mathbf{F}}_{\text{RF}}[m] \mathbf{F}_{\text{BB}}[m]. \quad (28)$$

Because of the reduced dimension of the baseband beamformer (i.e., $N_{\text{RF}} < N_T$), the BSA approach does not completely mitigate beam-squint. In other words, the beam-squint can be fully mitigated only if $\mathbf{F}_{\text{RF}}^\dagger \tilde{\mathbf{F}}_{\text{RF}}[m] = \mathbf{I}_{N_T}$ so that the resulting hybrid beamformer $\mathbf{F}_{\text{RF}} \tilde{\mathbf{F}}_{\text{BB}}[m]$ can be equal to $\tilde{\mathbf{F}}_{\text{RF}}[m] \mathbf{F}_{\text{BB}}[m]$, which requires $N_{\text{RF}} = N_T$. Nevertheless, the proposed approach provides satisfactory SE performance with beam-squint compensation for a wide range of bandwidth [12, 19]. Finally, the algorithmic steps of the proposed hybrid beamforming approach are presented in Algorithm 1, wherein we select the columns of the analog beamformer \mathbf{F}_{RF} from the near-field dictionary \mathbf{D} for $\ell = 1, \dots, N_{\text{RF}}$. In this process, the similarity between the columns of \mathbf{D} (i.e., $\mathbf{a}_T(\phi_p, r_p)$) and the residual beamformer (i.e., $\mathbf{F}_{\text{res}}[m]$) is performed. Since this process is iterated for $\ell = 1, \dots, N_{\text{RF}}$, its convergence is similar to the previous works [4, 27, 28].

IV. NUMERICAL EXPERIMENTS

We evaluated the performance of our hybrid beamforming technique in comparison with the fully digital (DF) ISAC

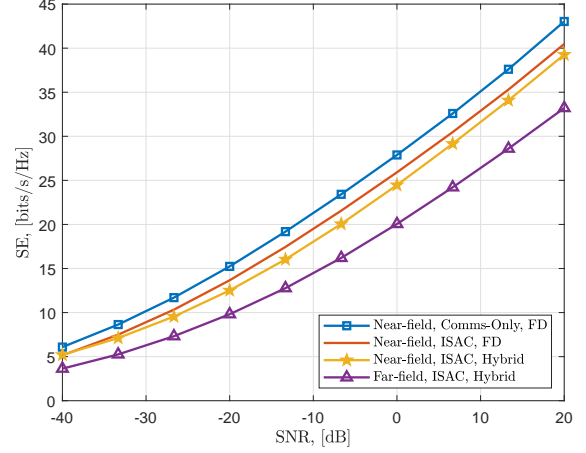


Fig. 2. SE performance versus SNR.

and communications-only beamformers as well as far-field-based design, in terms of SE, averaged over 500 Monte Carlo trials. The number of antennas at the BS and the user are $N_T = 128$ and $N_R = 16$, respectively. The carrier frequency and the bandwidth are selected as $f_c = 300$ GHz and $B = 20$ GHz, respectively, and the number of subcarriers is $M = 64$. The number of targets is $K = 3$, number of spatial paths is $L = 8$, number of RF chains is $N_{\text{RF}} = 8$ and the trade-off parameter is $\varepsilon = 0.5$. The dictionary grid size is obtained from $N_\phi = 100$, $N_r = 20$, yielding $N = N_\phi N_r = 2000$. Targets and path directions (ranges) are uniformly drawn at random from the intervals $[-\frac{\pi}{3}, \frac{\pi}{3}]$ ($[5, 30]$ m) [3].

Fig. 2 delineates the SE performance of the competing algorithms. We can see that the communications-only ($\varepsilon = 1$) FD beamformer provides the highest SE while the ISAC ($\varepsilon = 0.5$) FD beamformer provides marginally reduced SE due to power allocation for both communications and sensing tasks. The proposed beamforming approach exhibits performance closely resembling that of the FD beamformers. A significant performance degradation is also observed when the near-field model is overlooked in favor of the far-field array model.

Fig. 3 shows the SE performance against the bandwidth $B \in [0, 40]$ GHz. We can see that the proposed hybrid beamforming scheme achieves satisfactory SE performance up to $B \leq 30$ GHz, beyond which its performance slightly declines. This degradation arises because the BSA baseband beamformer's low-dimensional structure cannot adequately compensate for the beam-squint. Nevertheless, the hybrid beamforming scheme closely trails the performance of the FD beamforming and yields a substantial SE improvement compared to the far-field model.

V. SUMMARY

We introduced a hybrid beamforming scheme for THz-ISAC systems in near-field scenario. The analog beam-

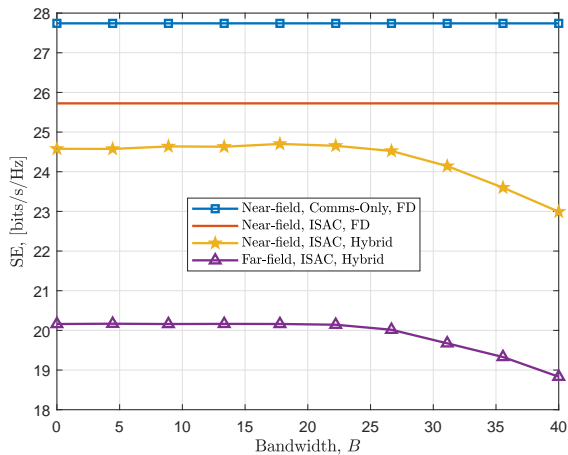


Fig. 3. SE performance versus bandwidth.

formers are designed based on a dictionary composed of near-field steering vectors. Then, the baseband and JRC beamformers are obtained. In order to cope with beam-squint problem in near-field scenario, we utilized the baseband beamformer to convey the impact of beam-squint from analog domain to baseband without requiring additional hardware components. As future work, we reserve to study a more challenging scenario, e.g., near-field ISAC joint precoder and combiner design.

REFERENCES

- [1] K. V. Mishra, M. R. B. Shankar, V. Koivunen, B. Ottersten, and S. A. Vorobyov, "Toward millimeter-wave joint radar communications: A signal processing perspective," *IEEE Signal Process. Mag.*, vol. 36, no. 5, pp. 100–114, 2019.
- [2] A. M. Elbir, K. V. Mishra, S. Chatzinotas, and M. Bennis, "Terahertz-band integrated sensing and communications: Challenges and opportunities," *arXiv preprint arXiv:2208.01235*, Aug. 2022.
- [3] A. M. Elbir, K. V. Mishra, and S. Chatzinotas, "Terahertz-band joint ultra-massive MIMO radar-communications: Model-based and model-free hybrid beamforming," *IEEE J. Sel. Top. Signal Process.*, vol. 15, no. 6, pp. 1468–1483, 2021.
- [4] R. W. Heath, N. González-Prelcic, S. Rangan, W. Roh, and A. M. Sayeed, "An overview of signal processing techniques for millimeter wave MIMO systems," *IEEE J. Sel. Top. Signal Process.*, vol. 10, no. 3, pp. 436–453, 2016.
- [5] A. M. Elbir, K. V. Mishra, S. A. Vorobyov, and R. W. Heath, "Twenty-Five Years of Advances in Beamforming: From convex and nonconvex optimization to learning techniques," *IEEE Signal Process. Mag.*, vol. 40, no. 4, pp. 118–131, Jun. 2023.
- [6] A. Alkhateeb and R. W. Heath, "Frequency selective hybrid precoding for limited feedback millimeter wave systems," *IEEE Trans. Commun.*, vol. 64, no. 5, pp. 1801–1818, 2016.
- [7] A. M. Elbir, W. Shi, A. K. Papazafeiropoulos, P. Kourtessis, and S. Chatzinotas, "Terahertz-Band Channel and Beam Split Estimation via Array Perturbation Model," *IEEE Open J. Commun. Soc.*, vol. 4, pp. 892–907, Mar. 2023.
- [8] B. Wang, M. Jian, F. Gao, G. Y. Li, and H. Lin, "Beam squint and channel estimation for wideband mmWave massive MIMO-OFDM systems," *IEEE Trans. Signal Process.*, vol. 67, no. 23, pp. 5893–5908, 2019.
- [9] A. M. Elbir and S. Chatzinotas, "BSA-OMP: Beam-Split-Aware Orthogonal Matching Pursuit for THz Channel Estimation," *IEEE Wireless Commun. Lett.*, vol. 12, no. 4, pp. 738–742, Feb. 2023.
- [10] F. Gao, B. Wang, C. Xing, J. An, and G. Y. Li, "Wideband beamforming for hybrid massive MIMO terahertz communications," *IEEE J. Sel. Areas Commun.*, vol. 39, no. 6, pp. 1725–1740, 2021.
- [11] L. You, X. Qiang, C. G. Tsinos, F. Liu, W. Wang, X. Gao, and B. Ottersten, "Beam squint-aware integrated sensing and communications for hybrid massive MIMO LEO satellite systems," *IEEE J. Sel. Areas Commun.*, vol. 40, no. 10, pp. 2994–3009, 2022.
- [12] A. M. Elbir, K. V. Mishra, A. Celik, and A. M. Eltawil, "Millimeter-Wave Radar Beamforming with Spatial Path Index Modulation Communications," in *2023 IEEE Radar Conference (RadarConf23)*. IEEE, May 2023, pp. 1–6.
- [13] E. Björnson, Ö. T. Demir, and L. Sanguinetti, "A Primer on Near-Field Beamforming for Arrays and Reconfigurable Intelligent Surfaces," in *2021 55th Asilomar Conference on Signals, Systems, and Computers*. IEEE, Oct. 2021, pp. 105–112.
- [14] X. Wei and L. Dai, "Channel Estimation for Extremely Large-Scale Massive MIMO: Far-Field, Near-Field, or Hybrid-Field?" *IEEE Commun. Lett.*, vol. 26, no. 1, pp. 177–181, Nov. 2021.
- [15] M. Cui and L. Dai, "Channel Estimation for Extremely Large-Scale MIMO: Far-Field or Near-Field?" *IEEE Trans. Commun.*, vol. 70, no. 4, pp. 2663–2677, Jan. 2022.
- [16] X. Zhang, Z. Wang, H. Zhang, and L. Yang, "Near-Field Channel Estimation for Extremely Large-Scale Array Communications: A model-based deep learning approach," *arXiv preprint arXiv:2211.15440*, Nov. 2022.
- [17] A. M. Elbir, W. Shi, K. V. Mishra, and S. Chatzinotas, "Federated Multi-Task Learning for THz Wideband Channel and DoA Estimation," *arXiv preprint arXiv:2207.06017*, Jul. 2022.
- [18] K. Dovelos, M. Matthaiou, H. Q. Ngo, and B. Bellalta, "Channel estimation and hybrid combining for wideband terahertz massive MIMO systems," *IEEE J. Sel. Areas Commun.*, vol. 39, no. 6, pp. 1604–1620, 2021.
- [19] A. M. Elbir, "A Unified Approach for Beam-Split Mitigation in Terahertz Wideband Hybrid Beamforming," *IEEE Trans. Veh. Technol.*, pp. 1–6, Apr. 2023.
- [20] A. M. Elbir, W. Shi, A. K. Papazafeiropoulos, P. Kourtessis, and S. Chatzinotas, "Near-Field Terahertz Communications: Model-Based and Model-Free Channel Estimation," *IEEE Access*, vol. 11, pp. 36409–36420, Apr. 2023.
- [21] A. M. Elbir, K. V. Mishra, and S. Chatzinotas, "NBA-OMP: Near-Field Beam-Split-Aware Orthogonal Matching Pursuit for Wideband THz Channel Estimation," in *ICASSP 2023 - 2023 IEEE International Conference on Acoustics, Speech and Signal Processing (ICASSP)*. IEEE, Jun. 2023, pp. 1–5.
- [22] Z. Wang, X. Mu, and Y. Liu, "Near-Field Integrated Sensing and Communications," *arXiv*, Feb. 2023.
- [23] H. Sarrieddeen, M.-S. Alouini, and T. Y. Al-Naffouri, "An overview of signal processing techniques for terahertz communications," *Proc. IEEE*, vol. 109, no. 10, pp. 1628–1665, 2021.
- [24] H. Yuan, N. Yang, K. Yang, C. Han, and J. An, "Hybrid beamforming for terahertz multi-carrier systems over frequency selective fading," *IEEE Trans. Commun.*, vol. 68, no. 10, pp. 6186–6199, 2020.
- [25] L. Yan, C. Han, and J. Yuan, "A Dynamic Array-of-Subarrays Architecture and Hybrid Precoding Algorithms for Terahertz Wireless Communications," *IEEE J. Sel. Areas Commun.*, vol. 38, no. 9, pp. 2041–2056, 2020.
- [26] M. Cui, L. Dai, Z. Wang, S. Zhou, and N. Ge, "Near-Field Rainbow: Wideband Beam Training for XL-MIMO," *IEEE Trans. Wireless Commun.*, p. 1, Nov. 2022.
- [27] O. E. Ayach, S. Rajagopal, S. Abu-Surra, Z. Pi, and R. W. Heath, "Spatially sparse precoding in millimeter wave MIMO systems," *IEEE Trans. Wireless Commun.*, vol. 13, no. 3, pp. 1499–1513, 2014.
- [28] A. Alkhateeb, G. Leus, and R. W. Heath, "Limited feedback hybrid precoding for multi-user millimeter wave systems," *IEEE Trans. Wireless Commun.*, vol. 14, no. 11, pp. 6481–6494, 2015.